Article

Characterization of low-cost inkjet printed-photonic cured strain gauges for remote sensing and structural monitoring applications

Juho Kerminen [1], Jenny Wiklund[2], Alp Karakoç [1,*] , Kalle Ruttik [1], Riku Jäntti [1], Hüseyin Yiğitler [1]

[1]   Department of Communications and Networking, Aalto University, 02150 Espoo, Finland; juho.kerminen@aalto.fi (J.K.); alp.karakoc@aalto.fi(A.K.); kalle.ruttik@aalto.fi (K.R.); riku.jantti@aalto.fi (R.J.); huseyin.yigitler@aalto.fi (H.Y.)
[2]   Department of Bioproducts and Biosystems, Aalto University, 02150 Espoo, Finland; jenny.wiklund@aalto.fi (J.W.)
*   Correspondence: alp.karakoc@aalto.fi

Abstract: In the present work, cost-effective strain gauges were fabricated by using inkjet printing and photonic curing on flexible and recyclable PET substrates. Ohmic resistance (a.k.a. DC resistance) (R_0) and complex electrical impedance (Z) as a function of test frequency were characterized, respectively, with the state-of-the-art electronic testing equipments. For the fabrication process, commercially available silver nanoparticle (AgNP) inks and printing substrates were used in order to eliminate any *apriori* ink processing. In order to validate the in-house cantilever beam measurement setup and devices, first, commercially available metallic foil strain gauges (with the provided gauge factor GF=2 by the manufacturer) were tested at different locations. Thereafter, the printed strain gauges were investigated with several repetitions at different measurement locations. The measurement results demonstrated an affordable, rapid and tailorable design and repeatable fabrication approach for strain gauges with $GF_{avg} \sim 6.6$, which has potential applications in remote sensing and structural monitoring applications.

check for
updates

1. Introduction

Strain gauges are electromechanical sensing devices created from thin conductive lines on top of a rigid or flexible substrate, which then attached to the measurement region [1,2]. The resistance, capacitance, impedance or piezoelectric characteristics of such devices change when the measurement region is subject to any source of deformation [3,4]. They can be fabricated by depositing metallic film onto substrates, photolithography, screen printing, aerosol or inkjet printing, to name a few [5–7]. Due to their cost-effectiveness, tailorable design, high bendability and stretchability, flexible printed strain gauges have been gaining grounds, e.g. in healthcare applications, wearable device technologies, structural health monitoring and intelligent packaging solutions [8–10].

Despite their pros and applicability, their electromechanical characteristics may vary a lot due to the fabrication processes, for which the micro-structural variations and fabrication repeatability play critical roles. For instance, in case of inkjet printing, which is based on deposition of ink droplets to create conductive traces with, e.g. of silver (Ag) or copper (Cu) nanoparticles (NPs), porosity, thickness and roughness at the boundaries of the traces have dominant effect on both electrical and mechanical characteristics of the designed devices [11–13]. To be able to improve such characteristics, e.g. strength and electrical conductivity, multiple layers of deposition and sintering methods have been proposed and widely applied in the literature [14,15]. It has been observed that sintering effectively agglomerate NPs by densifying and bonding them together while deposition of multiple layers increases the thickness of the conductive traces; hence, the electrical conductivity [16,17].

Traditionally, strain gauges are fabricated as metallic foils arranged in grid patterns and used in Wheatstone bridge configuration. The bridge usually measures the DC voltage

change on the strain gauge exposed to the applied loads F. For the metallic foil strain gauges, it is sufficient to characterize the initial reference ohmic resistance (a.k.a. DC resistance) R_0 and gauge factor (GF), which expresses the sensitivity of the strain gauge, as the correlation between the strain ε and the resistance change $\Delta R = R - R_0$ caused by ε with respect to R_0, i.e. $GF = \frac{\Delta R / R_0}{\varepsilon}$ [18]. For these strain gauges, $GF\sim 2$ is quite common while higher GF values have been achieved, e.g. $GF\sim 3$ and $GF\sim 5$ with inkjet printing by Rahman et al. and by Kravhcuk et al., respectively [19–21]. Nevertheless, variations exist in electrical characteristics of the printed strain gauges with the frequency shifts when they are deformed as a result of F. These changes can be explained with the uneven distribution of the conductive ink of the printed patterns resulting in microscopic inductance (L) and capacitance (C) changes subjected to F. Hence, this means that the printed strain gauge may function as resonant (LC) circuit with its specific resonant frequency ω_r. Therefore, in addition to R_0, frequency response ω and frequency dependent impedance of printed strain gauges $Z(\omega) = R(\omega) + jX(\omega)$, which is composed of resistance $R(\omega)$ and reactance $X(\omega)$, should be measured. Such characterization is especially useful for matching the impedance with the circuitry used in passive strain gauge measurement telemetry system, through which the strains can be remotely read [22–24].

In parallel with the current state of the art, a framework for the fabrication and characterization of printed strain gauge design was presented, which has prospective uses in remote sensing and structural monitoring. For the fabrication process, low-cost inkjet printing equipment was used and the effect of process parameters including number of deposited layers, i.e. trace height, and sintering, which was realized with photonic curing in the present study, on the conductivity was investigated. For the electromechanical characterization, a cantilever beam structure and an impedance analyzer were used to understand the frequency response of the printed strain gauges within the range of 0-500 MHz as function of ε due to F and to compute ω_r, which was around 200 MHz for the present design. Therefore, it was possible to compute reliable GF values by means of the defined frequency bandwidth of 49-50 MHz, which was a distant range from ω_r. For the validation of the characterization setup and comparison with the printed strain gauges, commercially available metallic foil strain gauges were used. The validation and comparison studies demonstrated that the printed strain gauges were promising with $GF\sim 6.6$ while the commercial ones were measured to have $GF\sim 1.8$, which is comparable with the provided $GF\sim 1.8$ by the manufacturer.

2. Methods

2.1. Design, fabrication of low-cost printed and photonic cured strain gauges

The strain gauge pattern as designed and represented in Fig.1 were parametrically created in Mathematica technical computing software and transferred as scalable vector graphics (.svg) to Inkscape open-source drawing software. The generated files were printed onto A4 size Mitsubishi NB-TP-3GU100 transparent polyethylene terephthalate (PET) special media, which has microporous Al_2O_3-PVA single-sided coating and sheet thickness of 135 ± 12 μm. The conductive ink used on the NB-TP-3GU100 special media was Mitsubishi NBSIJ-MU01 silver nanoparticle (AgNP) inkjet printer ink, which was also purchased from Mitsubishi Paper Mills Ltd. The ink was loaded to the black ink cartridge of Epson Stylus C88+ inkjet printer (5760 dpi x 1440 dpi resolution) (please, see Fig.2) with the following printer software settings: "Matte Paper - Heavyweight", "best photo" and "gray scale". For increasing the print quality and registration for the special media and AgNP ink, "High speed printing" option was set off.

Each printed gauge was composed of three printed layers, i.e. three passes over the same pattern, for the sake of better conductivity. For this purpose, a custom photonic curing system with 1500 W flash device was also assembled, the components of which were purchased from Xenon Flash Tubes LLC (www.xenonflashtubes.com), and implemented to sinter AgNPs for approximately 8 seconds immediately after the printing process was
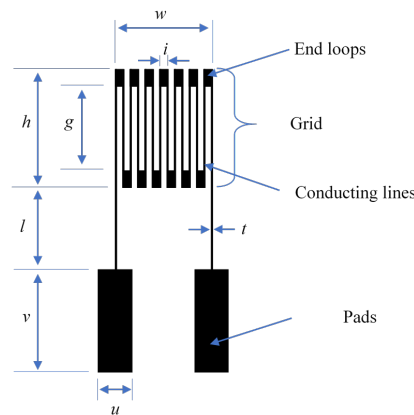
Parameter	Value
Number of conducting lines	14
Ink	Mitsubishi NBSIJ-MU01
	Ag nanoparticle content: 15%
	Ag nanoparticle diameter: 20 nm
Substrate	Mitsubishi NB-TP-3GU100
	Thickness: 135 μm
	Heat resistance: Max. 120 ºC
Printer/printer settings	Epson C88+ inkjet printer 5760 x 1440 dpi
	Matte, Heavyweight
	Grayscale
	Best Photo
	Low speed
Curing	Photonic curing, custom device
	Linear 400mm Reflector XFTR-L400C
	(1500W XenonFlash)
	15 seconds for each layer
Number of printed layers	3
Grid line (trace) thickness, b	~0.4 micron [1]
Gage length, g	27 mm
Grid height, h	34 mm
End loop width, i	2 mm
Transition, l	15 / 20 / 25 mm
Grid width, w	20 mm
Grid line (trace) width, t	~ 0.35 mm
Pad width, u	7 mm
Pad height, v	21 mm

Figure 1. Geometric and fabrication process parameters of the inkjet printed strain gauge.

over for each layer. The conductivity was observed to be drastically improved, both R_0 and microscopic structure of which were investigated as provided in the Results section.

For R_0 measurements, TENMA 72-7745 multimeter was used while 6.3 MP Swiftcam microscope digital camera apparatus was used for the microscopic analysis. In order to measure the printed trace height and generate the height maps, L&W Optitopo surface roughness measurement device was used as depicted in Fig.2. Through this device, a pattern of shadows was created by illuminating the sample surface from a small angle. Thereafter, by utilizing two images of the same area illuminated from opposite sides, the height maps for the printed strain gauges were generated in μm scale. The measurement area was taken as 32 mm×32 mm, which is the maximum range achieved with L&W Optitopo, and the resolution and bandpass were 15.625 μm and 0.01-0.5 mm, respectively. In order to analyze the height uniformity, the height profiles were measured over 3 rows (top-center-bottom) on the grids of the printed strain gauges.

2.2. Experiment setup and measurement system for characterization

In order to evaluate the performance and understand the characteristics of the the printed strain gauges, a slender cantilever beam as schematized in Fig. 3 was built so that only bending moments (eliminating the shear) were taken to be the dominant source of deformation. Here, l is the distance between the fixed and F referring to the applied load, x, b and h are the distance between the fixed end and strain gauge center, beam breadth and height, respectively. At the free end of the beam, a 3D printed plate was attached with a single screw to provide an easy way of applying load F at the specified distance $l=$ 390 mm. For this purpose, a set of calibration weights was used, and deflections, strains and electrical characteristics of the printed strain gauges and the commercial reference gauges (RS PRO 4 mm 120-Ω metallic foil strain gauge with the gauge factor GF=2) at two different beam locations, x=120 mm and 170 mm, were measured (please, see Fig.3).

The conductive pads of the printed strain gauges were firmly attached to 10 cm wires with conductive copper tape. Thereafter, the strain gauges were taped to the measurement location x and pressed with a support plate in order to have a firm grip of the strain gauge and provide correct bending and stretch/contraction over it. The wires were then connected to a Hioki IM9202 test fixture as shown in Fig. 2(c), which was then connected to IM9201 test head used by the Hioki IM7587 impedance analyzer for measuring R and Z of the strain gauge. The measurements were carried out by sweeping a signal frequency range of 1-120 MHz with LCR-mode on, which was repeated ten times to obtain the average and the standard deviation. The shortest possible frequency interval of 0.1 MHz provided by
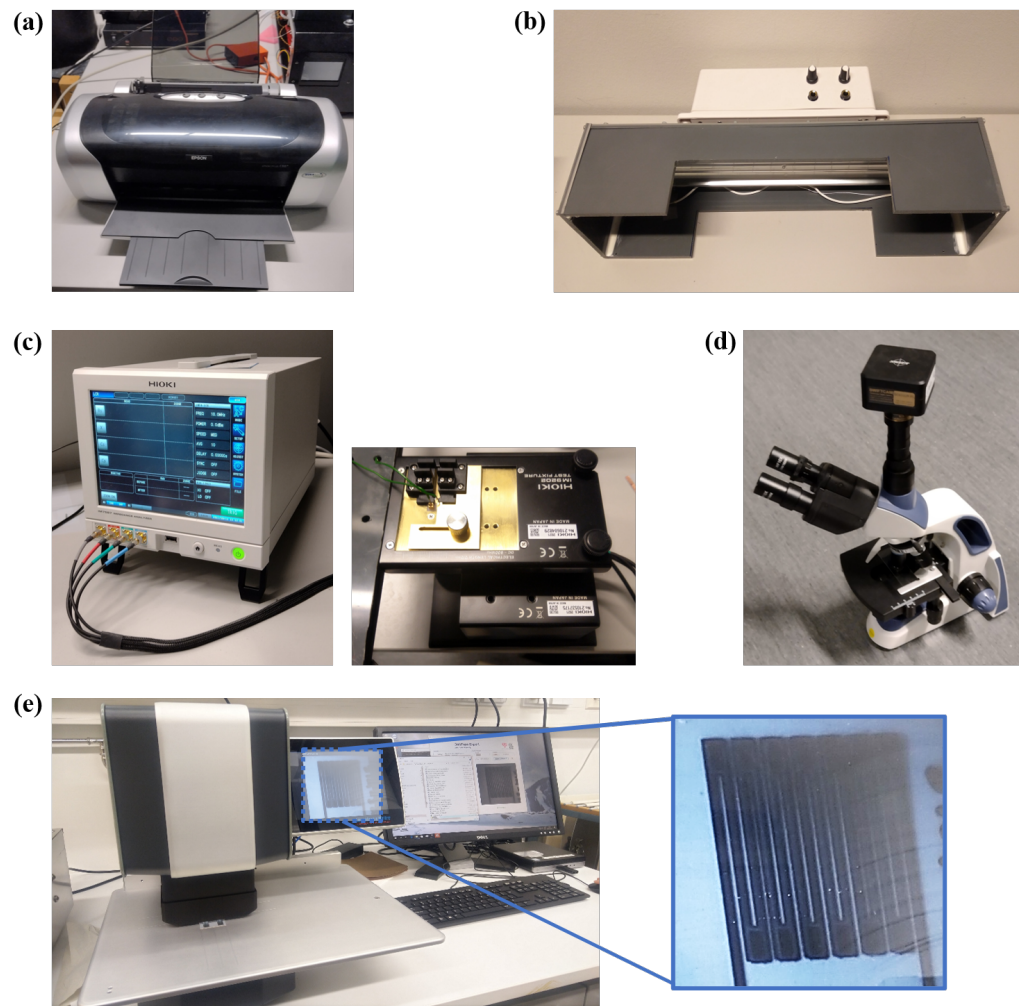
Figure 2. Printing and measurement devices: (a) Epson Stylus C88+ printer, (b) In-house photonic curing device, (c) HIOKI IM7587 impedance analyzer and IM9202 test fixture, (d) light microscope equipped with 6.3 MP Swiftcam digital camera, (e) height measurement for printed traces with L&W Optitopo system.

the device was used while samples were taken with the impedance analyzer application provided by Hioki capable of sweeping and saving the data as .csv file. In all the tests, applied load F was adjusted in order to provide the beam deflections of δ={0, 0.3, 0.6, 0.9 , 1.2, 1.5, 1.8, 2.1, 2.4} mm with a tolerance of 0.05 mm at the measurement locations, which were later converted into strains ε by using the formula sets provided in the Appendix. As shown in Fig.3, an RS Pro electronic digital indicator gauge with $\pm$ 0.02 mm accuracy and 25 mm range was used for the deflection measurements.
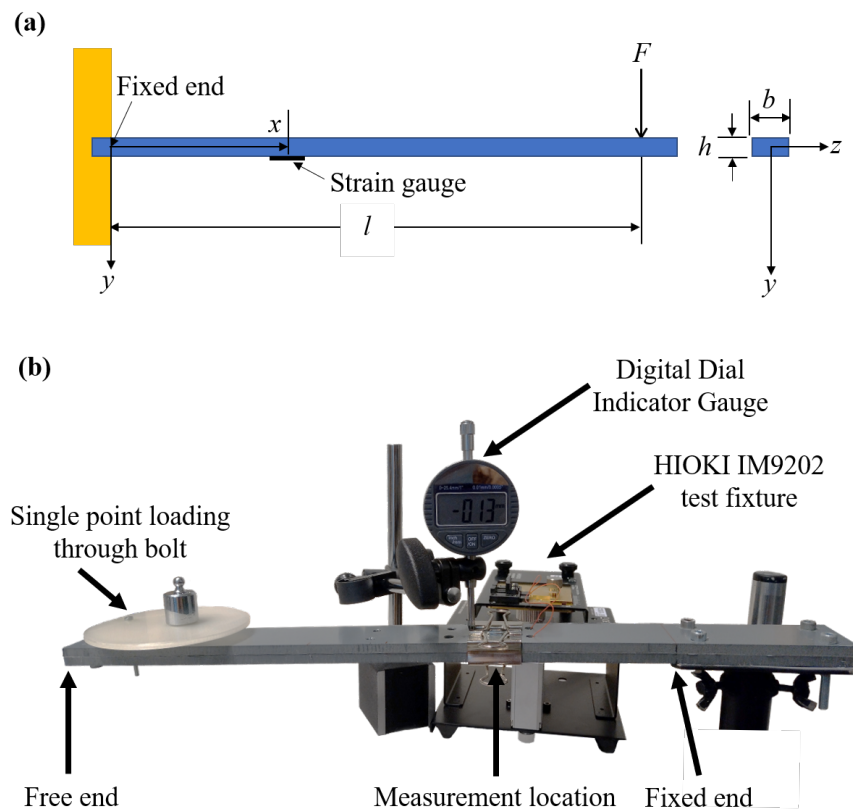
Figure 3. Cantilever beam: (a) schematic diagram, (b) setup with the test fixture and digital dial indicator gauge.

3. Results and discussion
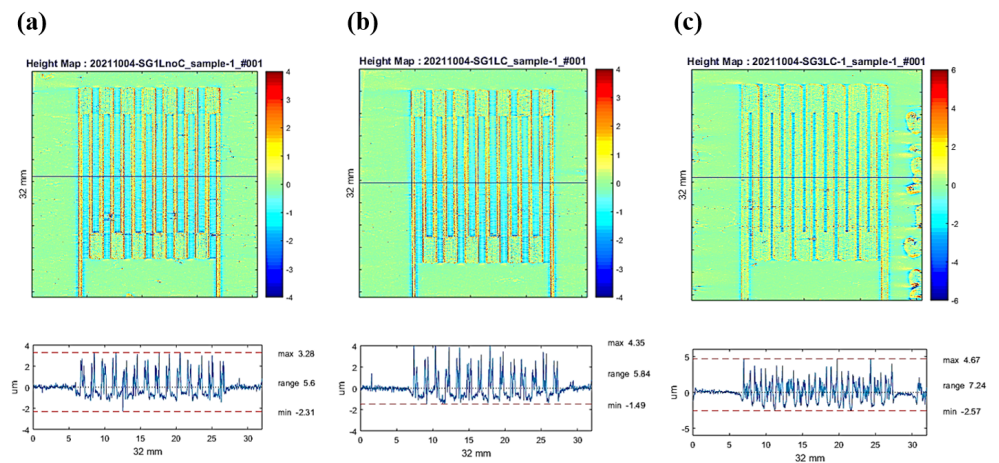### 3.1. Effects of printed layers and photonic curing

Figure 4. Effect of printed layers and curing on the strain gauge height profiles: (**a**) one layer of print no curing, (**b**) one layer of print with curing, (**c**) three layers of print with curing after each layer. The scanned area is 32 mm x 32 mm while the height profiles are represented in μm scale, which were obtained by scanning the center rows of the strain gauge grids.
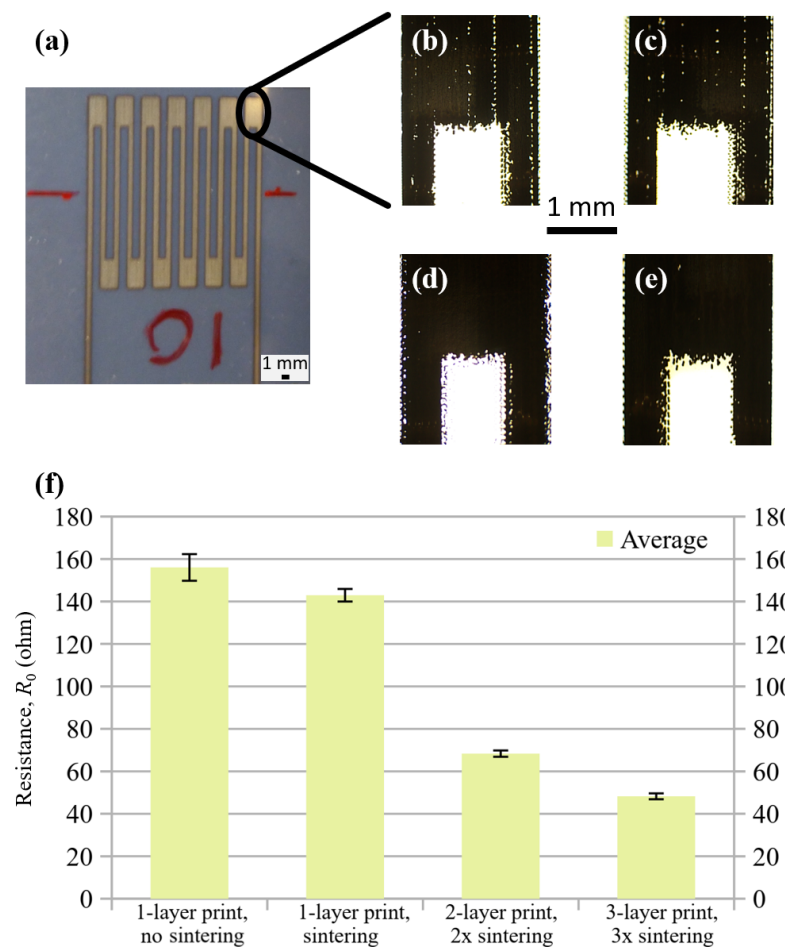
Figure 5. Printed strain gauge and light microscope images showing the morphological changes due to photonic curing and number of printed layers: (**a**) digital still, (**b**) light microscope image for one layer of print without photonic curing, (**c**) one layer of print and photonic curing, (**d**) two layers of print and photonic curing, (**e**) three layers of print and photonic curing, (**f**) impact of multiple layers and curing on the ohmic resistance R_0 of printed strain gauge.

In order to understand the conductivity changes with respect to the fabrication parameters and provide repeatable process solutions, a set of measurements were carried out. Through these measurements, the effects of number of printed layers and photonic curing on the printing quality and resistance of strain gauges were analyzed. For this purpose, one, two and three layers of AgNP ink were printed onto the substrate, respectively, where the sintering was carried out with photonic curing of 1500 W for approximately 8 seconds. The height profiles depicted in Fig. 4 demonstrates that both printed layers and curing have positive effect on the trace height. However, as a negative effect, the increase in number of printed layers caused spreading of the ink; thus, undesired increase in trace width. In addition to the height profile measurements, as seen in the microscope images of Fig. 5, photonic curing combined with multiple layers of printing was also observed to provided more consistent and denser traces. For instance, Fig. 5(b) for one layer of print without any sintering shows that some of the deposited ink droplets were not connected to the agglomerate. As a result of these unconnected droplets of the printed structure, the resistance was observed to be as high as $R_0 = 160\ \Omega$ for the designed and printed strain gauges. However, after printing and curing the second layer, there was a drastic reduction in the resistance of $R_0 = 65\ \Omega$ on average, which continued to drop to $R_0 = 45\ \Omega$ on average with additional third layer and photonic curing (please, see Fig. 5 (f)). Interestingly, the resulting resistance of three-layer strain gauge is close to 50 Ω that is common standard for

matching different circuits [25]. In addition, the effect of adding more than three layers on the conductivity was obtained to be negligible; thus, three printed layers with photonic curing was taken as the fabrication parameters for the present designed strain gauges.
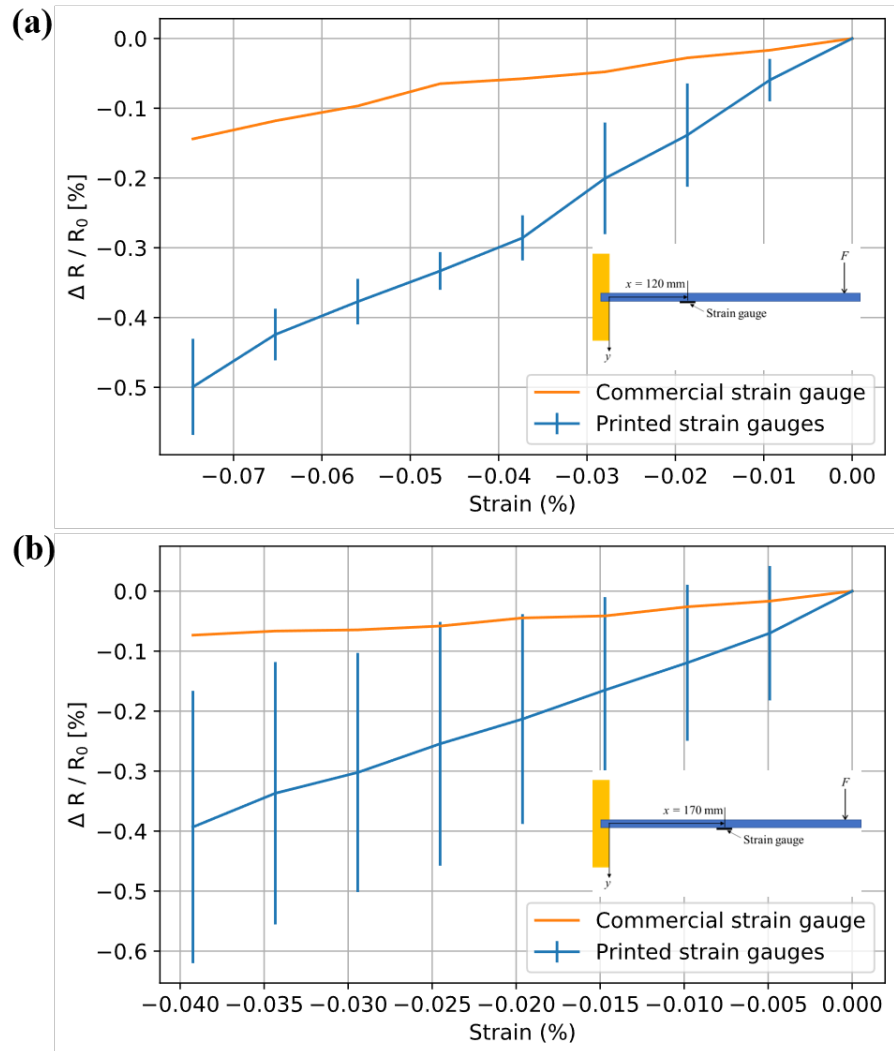
3.2. Gauge factor GF

Figure 6. Resistance change ΔR with respect to R_0 of the printed strain gauges as a function of strain within the 49-50 MHz bandwidth: (a) at x=120 mm and (b) at x=170 mm. Error bars refer to the standard deviation while the straight lines represent the mean values.

In order to investigate the accuracy of the built setup and determine the *GF* of the printed strain gauges, measurements were carried out at two different locations on the cantilever beam, i.e. x=120 mm and x=170 mm (please, see Fig.) Fig.3. As the initial step, frequency bandwidth was set to 49-50 MHz for *GF* measurements because of great impedance variations near ω_r~200 MHz (as elaborated in the following sections). The chosen range provided stable results for *GF* and beam deflection-impedance correlation.

For the measurement setup and device validation, the measurements were conducted by using the commercially available metallic foil strain gauges with the provided *GF*~2 by the manufacturer datasheet. As a result of the measurements, *GF* was determined to be *GF*~1.8, showing 10% measurement setup and device error. For the printed strain gauges, *GF*~6.6±0.3 and *GF*~6.6±0.9 were measured for x=120 mm and x=170 mm, respectively. This demonstrates that the printed strain gauges provide repeatable results at different measurement locations with varying beam deflections. It is also noteworthy that the

printed strain gauges were obtained to have higher sensitivity when compared with the commercial strain gauge measurements. This also shows the application potentials of the the printed strain gauges, e.g. in detecting tiny vibrations and daily movements of the human body, which can be cumbersome with the conventional gauges [26].

3.3. Impedance Z and frequency dependency

The resistance and reactance of the printed strain gauges are depicted in Fig. 7. All three strain gauges have relatively close frequency responses with the resonant frequency ω_r around 200 MHz. At ω_r, the resistance is at its highest value while the reactance changes the phase, which brings forth the impact of the fabrication/printing related differences. As seen in Fig. 7, close to ω_r, all the fabrication/printing originated variations are amplified, which makes it more difficult to control the uniformity of the strain gauge behaviour. On the other hand, all the strain gauge have relatively close behaviour well below ω_r.

In Figs. 8a and 9a, resistance change, ΔR, and reactance change, ΔX of a printed strain gauge, which can be elaborated as the differences between the values measured for deformed configuration caused by ε and initial configuration, are provided for 800 MHz bandwidth. Below ω_r, ΔR has negative dependency while above it is vice versa. The closer the frequency is to the resonant frequency, the higher is the sensitivity to the strain. Besides, as seen in Fig. 7, variances between the different gauges were observed to be amplified at around ω_r. For sufficiently low frequency below ω_r, strain gauge resistance has systematic dependency on ε, which is depicted in the magnified portion of Fig 8b. This indicates that a printed strain gauge does not have to operate only on DC frequency but can also operate on some higher frequency. Around ω_r and above, it was deduced that the printed strain gauge has to be calibrated. Such calibration is needed in order to remove printing related variations between the strain gauges and to identify whether there exists negative or positive ε dependency at particular frequency.

Nonetheless, the results in Fig. 9a indicates that the printed strain gauges can measure deflections not only by ΔR but also by ΔX. Interestingly, ΔX has higher strain sensitivity above ω_r. Similar to the ΔR measurements, the ΔX frequency response is mostly monotonous below ω_r, which was similar to the trend obtained for the ΔR measurements (please, see Figs. 9a and Fig 8b). However, it is also noteworthy that the ΔX values of the printed strain gauges subjected to bending were observed to be changing from positive to negative around 45 MHz, which requires attention in case of reactance based strain measurements.

In addition to the printed strain gauges, comparative frequency dependent investigations for ΔR and ΔX was also carried out with commercially available strain gauges, the plots of which are presented in Fig. 10. For these particular strain gauges, the range of bending dependency was obtained to be in much more smaller range than the one for the printed strain gauges. Similar to the printed strain gauges, the results for the commercial strain gauges in Fig. 10 indicates that there is negative bending dependency of both ΔR and ΔX.
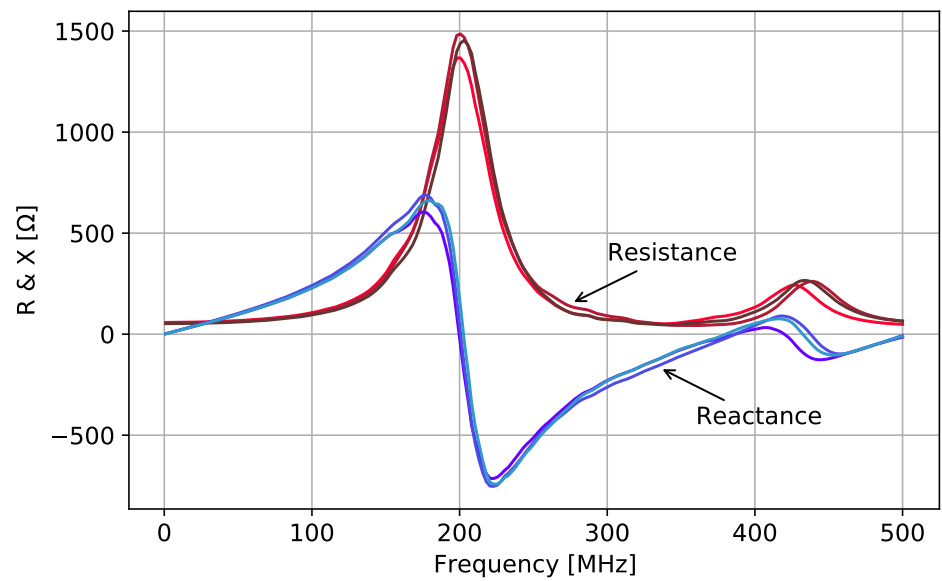
Figure 7. Resistance R and reactance X measurements for three printed strain gauges in unloaded initial configuration, i.e. no bending.
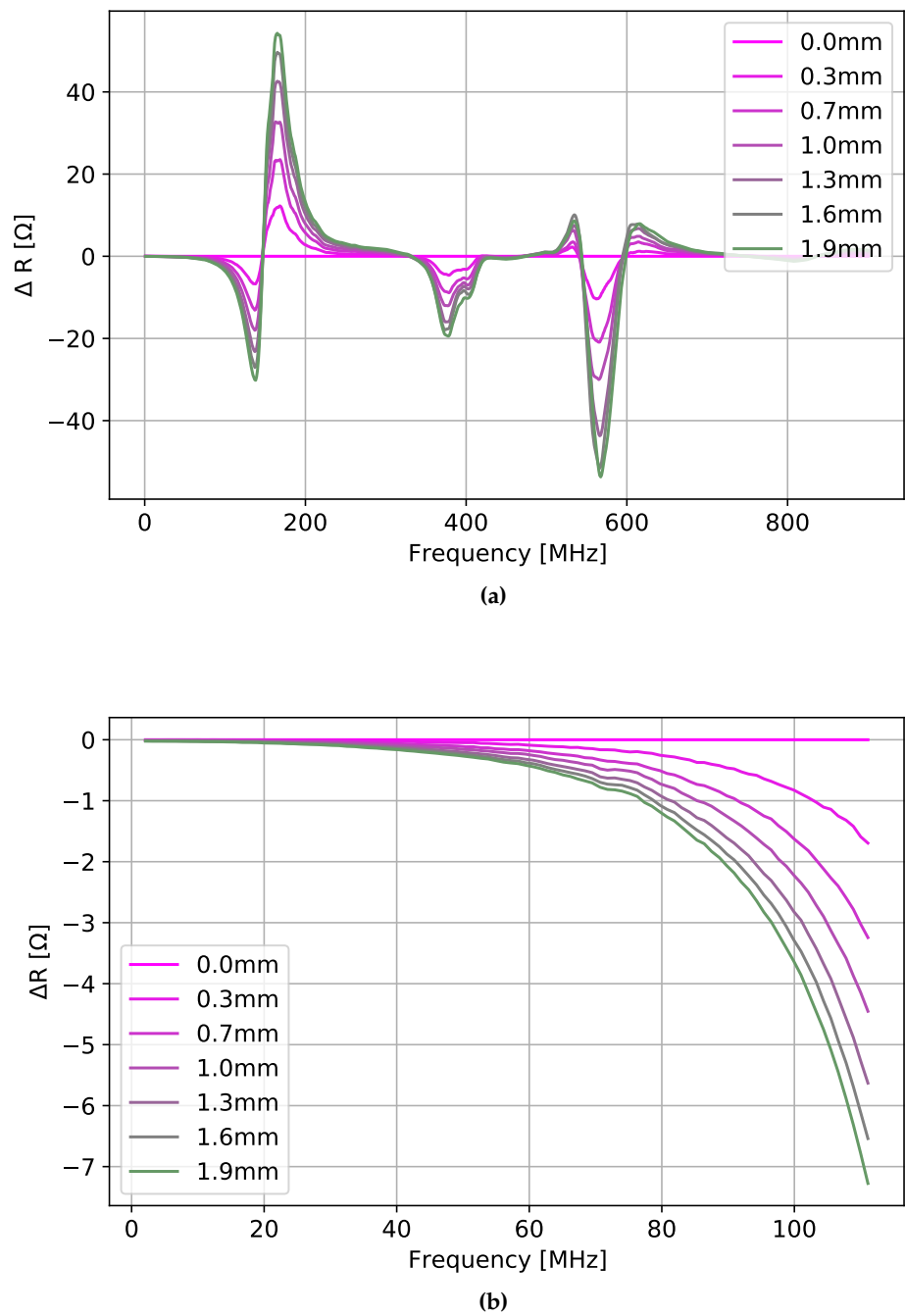
(a)

(b)

Figure 8. Resistance change ΔR of one strain gauge under deflection: (a) the whole measured bandwidth, (b) restrained bandwidth.

(a)

(b)

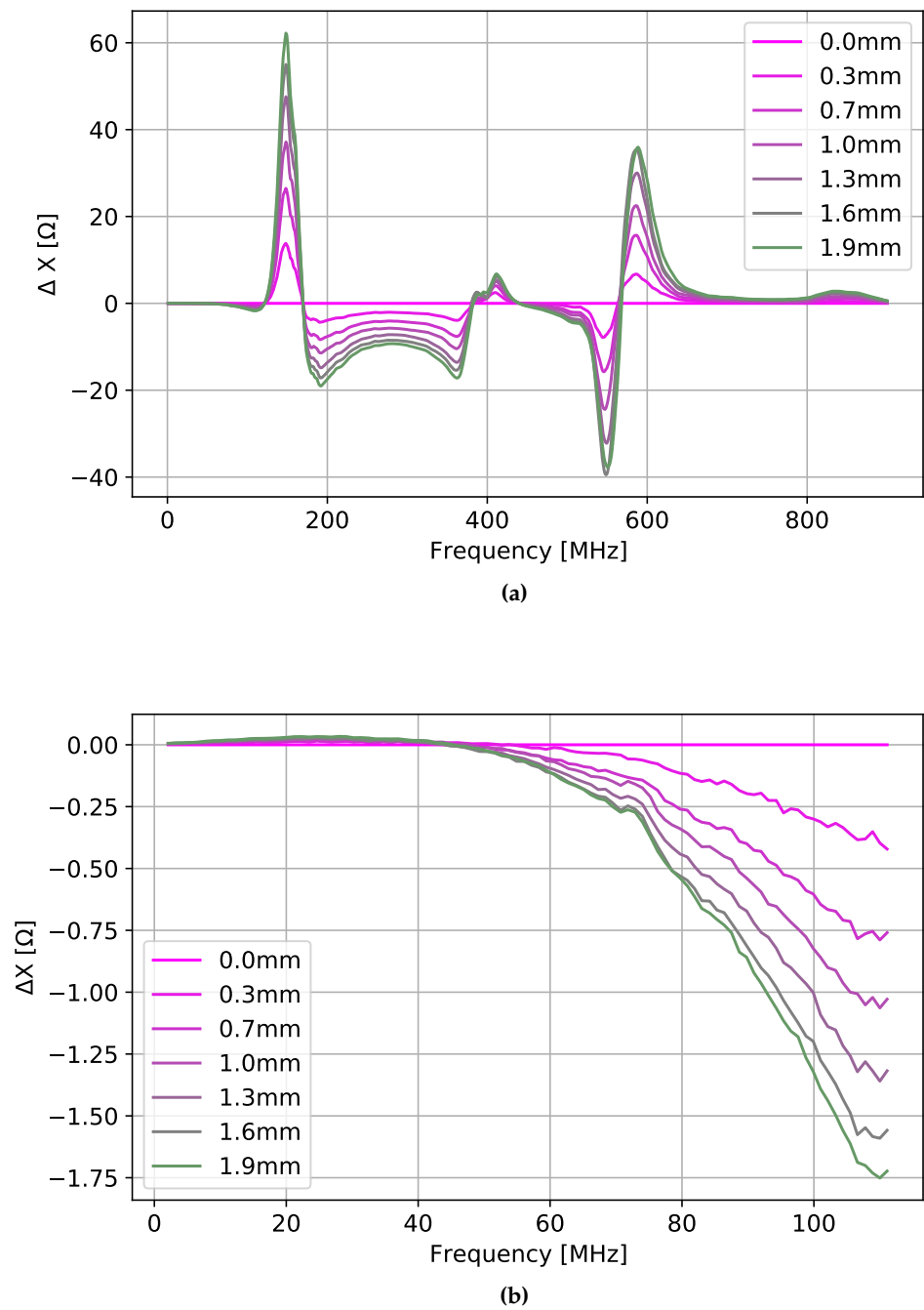**Figure 9.** Reactance change ΔX of one strain gauge under deflection: (a) the whole measured bandwidth, (b) restrained bandwidth.
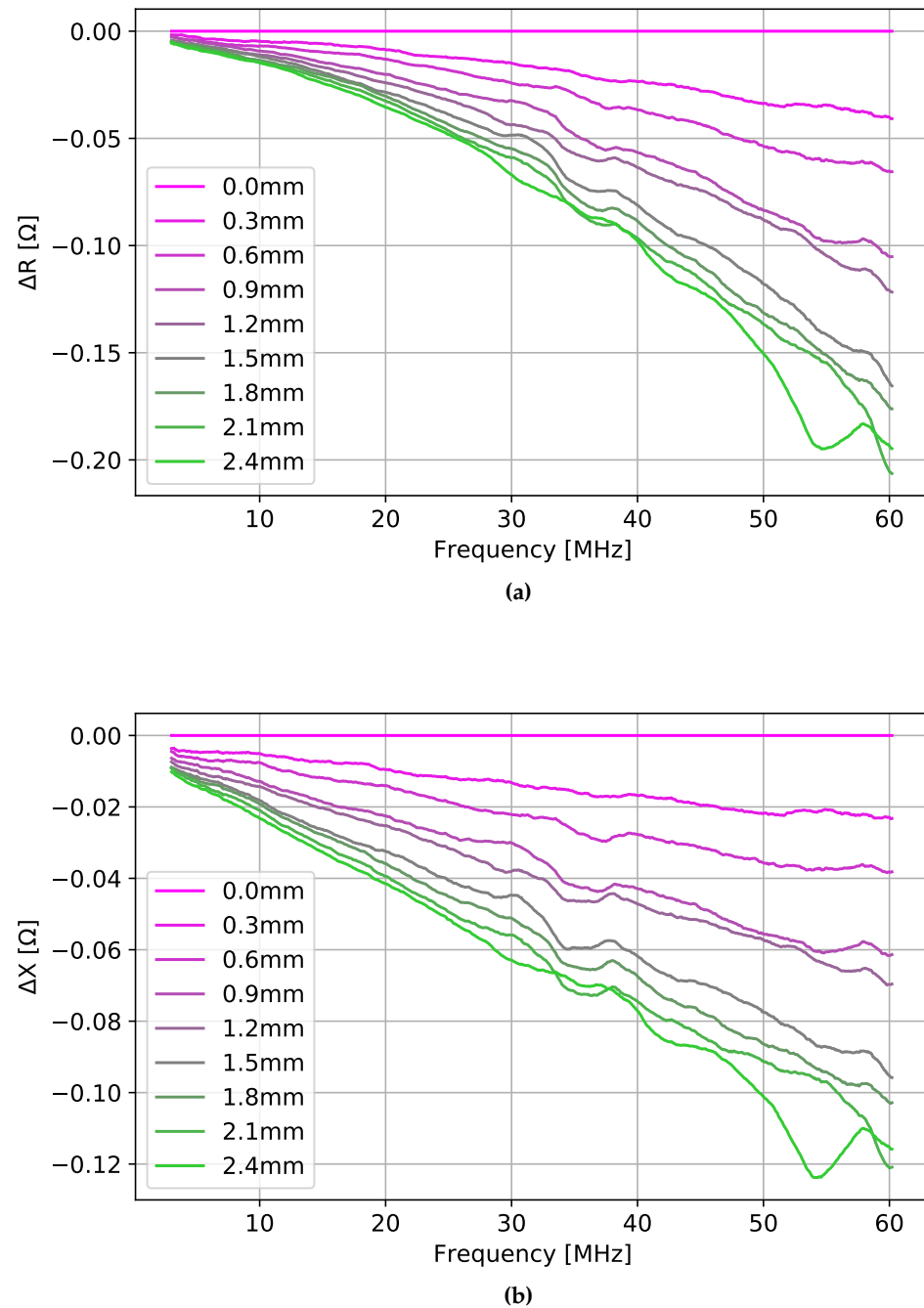
(a)

(b)

Figure 10. Commercial strain gauge at x=170 mm position: (a) resistance change ΔR, (b) reactance change ΔX.

4. Conclusion

The present study provided a framework for the fabrication and characterization of low-cost inkjet-printed strain gauges, ΔR and ΔX of which vary with the applied load F and frequency. The printing parameters such as number of printed layers and curing were found out to have positive effects on the conductivity. For instance, R_0=45 Ω and $GF{\sim}6.6$ (within the frequency bandwidth of 49-50 MHz) on average for three printed layers with photonic curing were achieved. Therefore, these affordable and easy-to-design printed strain gauges can be an alternative to the commercially available ones with similar dimensions but higher resistance (R_0=120 Ω) and lower gauge factors ($GF{\sim}2$). In addition,

the printed strain gauges functioning as resonant (LC) circuit with its specific resonant frequency ω_r can be used as flexible and tailorable solutions for remote sensing and structural monitoring applications.

Author Contributions

All authors contributed to the manuscript while H.Y. conceptualized; J.K., J.W., A.K., K.R. and R.J. coordinated the measurements, manuscript writing and editing processes. The authors gratefully acknowledge the technical assistance of Timi Lehtola and Juhapekka Hietala. All the authors have agreed to the present version of the manuscript.

Funding

Data Availability Statement

Data sharing not applicable.

Conflicts of interest

The authors declare no conflict of interest.

References

1. Fujimoto, K.T.; Watkins, J.K.; Phero, T.; Litteken, D.; Tsai, K.; Bingham, T.; Ranganatha, K.L.; Johnson, B.C.; Deng, Z.; Jaques, B.; Estrada, D. Aerosol jet printed capacitive strain gauge for soft structural materials. *npj Flexible Electronics* **2020**, *4*, 2397–4621. doi:10.1038/s41528-020-00095-4.
2. Mitterlehner, T.; Beisteiner, C.; Polixmair, M.; Steinbichler, G. Injection Molding Parts with Integrated All-Inkjet Printed Strain Gauge for Condition Monitoring. ANTEC® 2018 - Proceedings of the Technical Conference & Exhibition, Orlando, FL, May 7-10, 2018. Society of Plastics Engineers, 2018.
3. Yi, Y.; Wang, B.; Bermak, A. A low-cost strain gauge displacement sensor fabricated via shadow mask printing. *Sensors* **2019**, *19*, 4713.
4. Kim, J.; Kim, K.; Ham, S.W.; Bae, N.H.; Park, M.K.; Min, N.K. A hydrogen pressure sensor based on bulk-micromachined silicon strain gauges. *Procedia Engineering* **2016**, *168*, 790–793.
5. Shakeel, M.; Khan, W.A.; Rahman, K. Fabrication of cost effective and high sensitivity resistive strain gauge using DIW technique. *Sensors and Actuators A: Physical* **2017**, *258*, 123–130.
6. Thompson, B.; Yoon, H.S. Aerosol-printed strain sensor using PEDOT: PSS. *IEEE Sensors Journal* **2013**, *13*, 4256–4263.
7. Andò, B.; Baglio, S.; La Malfa, S.; L'Episcopo, G. All inkjet printed system for strain measurement. SENSORS, 2011 IEEE. IEEE, 2011, pp. 215–217.
8. Mantysalo, M.; Pekkanen, V.; Kaija, K.; Niittynen, J.; Koskinen, S.; Halonen, E.; Mansikkamaki, P.; Hameenoja, O. Capability of inkjet technology in electronics manufacturing. 2009 59th Electronic Components and Technology Conference. IEEE, 2009, pp. 1330–1336.
9. Ando, B.; Baglio, S. All-inkjet printed strain sensors. *IEEE Sensors Journal* **2013**, *13*, 4874–4879.
10. Wiklund, J.; Karakoç, A.; Palko, T.; Yiğitler, H.; Ruttik, K.; Jäntti, R.; Paltakari, J. A Review on Printed Electronics: Fabrication Methods, Inks, Substrates, Applications and Environmental Impacts. *Journal of Manufacturing and Materials Processing* **2021**, *5*, 89.
11. Cummins, G.; Desmulliez, M.P. Inkjet printing of conductive materials: a review. *Circuit World* **2012**, *38*, 193–213. doi:10.1108/03056121211280413.
12. Özkan, M.; Dimic-Misic, K.; Karakoc, A.; Hashmi, S.G.; Lund, P.; Maloney, T.; Paltakari, J. Rheological characterization of liquid electrolytes for drop-on-demand inkjet printing. *Organic Electronics* **2016**, *38*, 307–315.
13. Özkan, M.; Hashmi, S.G.; Halme, J.; Karakoc, A.; Sarikka, T.; Paltakari, J.; Lund, P.D. Inkjet-printed platinum counter electrodes for dye-sensitized solar cells. *Organic Electronics* **2017**, *44*, 159–167.
14. Roshanghias, A.; Krivec, M.; Baumgart, M. Sintering strategies for inkjet printed metallic traces in 3D printed electronics. *Flexible and Printed Electronics* **2017**, *2*, 045002.

15. Kuroda, K.; Nakako, H.; Inada, M.; Noudou, T.; Kumashiro, Y. Development of copper materials and processing for printed electronics. *Transactions of The Japan Institute of Electronics Packaging* **2012**, *5*, 20–25.
16. Saleh, E.; Vaithilingam, J.; Tuck, C.; Wildman, R.; Hague, R.; Ashcroft, I.; Dickens, P. 3D inkjet printing of conductive structures using in-situ IR sintering. 2015.
17. German, R. Thermodynamics of sintering. In *Sintering of advanced materials*; Elsevier, 2010; pp. 3–32.
18. Kitzing, H. A solid base for precision strain gauge measurements. Proceedings of XVI. IMEKO World Congress, Vienna, Austria, 2000, pp. 405–408.
19. Heckmann, U.; Bandorf, R.; Gerdes, H.; Lübke, M.; Schnabel, S.; Bräuer, G. New materials for sputtered strain gauges. *Procedia Chemistry* **2009**, *1*, 64–67.
20. Rahman, M.T.; Moser, R.; Zbib, H.M.; Ramana, C.; Panat, R. 3D printed high performance strain sensors for high temperature applications. *Journal of Applied Physics* **2018**, *123*, 024501.
21. Kravchuk, O.; Reichenberger, M. Properties and long-term behavior of nanoparticle based inkjet printed strain gauges. *Journal of Materials Science: Materials in Electronics* **2016**, *27*. doi:10.1007/s10854-016-5207-9.
22. Bona, M.; Sardini, E.; Serpelloni, M.; Andò, B.; Lombardo, C.O. Study on Impedance Behavior of a Telemetric System Operating with an Inkjet-Printed Resistive Strain Gauge. Sensors; Andò, B.; Baldini, F.; Di Natale, C.; Marrazza, G.; Siciliano, P., Eds.; Springer International Publishing: Cham, 2018; pp. 258–266.
23. Bona, M.; Sardini, E.; Serpelloni, M.; Andò, B.; Lombardo, C.O. Study on a telemetrie system that works with an inkjet-printed resistive strain gauge. 2016 IEEE Sensors Applications Symposium (SAS), 2016, pp. 1–6. doi:10.1109/SAS.2016.7479869.
24. Cheng, X.; Yu, Y.; Wang, L.; Sun, C.; Tian, G. Wireless stress measurement on metal surface based on passive integrated RFID sensor tag. 2021 IEEE International Instrumentation and Measurement Technology Conference (I2MTC). IEEE, 2021, pp. 1–6.
25. Yarman, B. A Simplified Real Frequency Technique for Broadband Matching Complex. *IIMBO* **1982**, *43*, 529.
26. Yan, W.; Fuh, H.R.; Lv, Y.; Chen, K.Q.; Tsai, T.Y.; Wu, Y.R.; Shieh, T.H.; Hung, K.M.; Li, J.; Zhang, D.; others. Giant gauge factor of Van der Waals material based strain sensors. *Nature communications* **2021**, *12*, 1–9.
27. Young, W.C.; Budynas, R.G.; Sadegh, A.M. *Roark's formulas for stress and strain*; McGraw-Hill Education, 2012.

Appendix

Based on the provided annotations for cantilever beam geometry and applied point load in Fig. 3, the relationship between the beam deflection and strain at the strain gauge location can be expressed as follows [27]

Deflection at the strain gauge location, $x \in \mathbb{R}^+$:

$$\delta = \frac{Px^2}{6EI}(3l - x) \tag{1}$$

Point load in terms of deflection:

$$P = \delta \frac{6EI}{x^2(3l - x)} \tag{2}$$

Stress at x:

$$\sigma = \frac{My}{I} = \frac{P(l-x)y}{I} = P\frac{(l-x)h}{2I} \tag{3}$$

Stress in terms of deflection:

$$\sigma = \delta \frac{3E}{x^2(3l - x)}(l - x)h \tag{4}$$

Stress - strain relationship (assuming linear elasticity):

$$\varepsilon = \frac{\sigma}{E} \tag{5}$$

Strain in terms of deflection at x:

$$\varepsilon = \delta \frac{3}{x^2(3l - x)}(l - x)h \tag{6}$$